

Contrast enhancement for portal images by combination of subtraction and reprojection processes for Compton scattering

Masatsugu Hariu | Yuhi Suda | Weishan Chang | Atsushi Myojoyama | Hidetoshi Saitoh

Graduate School of Human Health Sciences, Tokyo Metropolitan University, Tokyo, Japan

Author to whom correspondence should be addressed. Masatsugu Hariu
E-mail: hariu-masatsugu@ed.tmu.ac.jp;
Telephone: +81338191211

Abstract

For patient setup of the IGRT technique, various imaging systems are currently available. MV portal imaging is performed in identical geometry with the treatment beam so that the portal image provides accurate geometric information. However, MV imaging suffers from poor image contrast due to larger Compton scatter photons. In this work, an original image processing algorithm is proposed to improve and enhance the image contrast without increasing the imaging dose. Scatter estimation was performed in detail by MC simulation based on patient CT data. In the image processing, scatter photons were eliminated and then they were reprojected as primary photons on the assumption that Compton interaction did not take place. To improve the processing efficiency, the dose spread function within the EPID was investigated and implemented on the developed code. Portal images with and without the proposed image processing were evaluated by the image contrast profile. By the subtraction process, the image contrast was improved but the EPID signal was weakened because 15.2% of the signal was eliminated due to the contribution of scatter photons. Hence, these scatter photons were reprojected in the reprojection process. As a result, the tumor, bronchi, mediastinal space and ribs were observed more clearly than in the original image. It was clarified that image processing with the dose spread functions provides stronger contrast enhancement while maintaining a sufficient signal-to-noise ratio. This work shows the feasibility of improving and enhancing the contrast of portal images.

PACS

87.57.C-, 87.57.cj, 87.57.cm

KEY WORDS

EPID, image contrast, Monte Carlo simulation, portal image, scatter correction

1 | INTRODUCTION

Image-guided radiation therapy (IGRT) employs imaging to maximize geometric accuracy and precision during a treatment session. Various systems, e.g., in-treatment-room computed tomography (CT-on-rails),

kilovoltage cone beam CT (kV-CBCT), portal imaging and megavoltage cone beam CT (MV-CBCT) are currently available for the IGRT.^{1,2}

CT-on-rails and kV-CBCT can provide superior soft tissue contrast and anatomical information while an additional kV X-ray source and extra detector are required. The coordinates of two isocenters

This is an open access article under the terms of the Creative Commons Attribution License, which permits use, distribution and reproduction in any medium, provided the original work is properly cited.

© 2017 The Authors. *Journal of Applied Clinical Medical Physics* published by Wiley Periodicals, Inc. on behalf of American Association of Physicists in Medicine.

of kV imaging and treatment beam must be adjusted carefully for correct patient repositioning. Hence, quality assurance (QA) is more complex than that for MV imaging.^{3,4} MV portal and MV-CBCT imaging can be performed in identical geometry with the treatment beam so that accurate geometric information can be provided.^{5,6} However, MV imaging suffers from poor image contrast due to the lower difference of X-ray attenuation and larger Compton scattering compared with kV imaging.^{7,8}

Scatter correction methods that comprise scatter estimation and compensation have been reported.^{9,10} The beam-scatter-kernel (BSK) superposition approach is the most promising in the scatter estimation method with respect to the computational efficiency.¹¹ The BSK is generally obtained using water rather than heterogeneous mediums and consequently it causes over- or underestimation of scatter photons.

In this work, the scatter estimation was performed in detail by Monte Carlo (MC) simulation based on patient CT data. Additionally, an original image processing algorithm was proposed for the scatter compensation. In this process, scatter photons were eliminated and reprojected as primary photons on the electronic portal imaging device (EPID). By the combination of the MC simulation and the proposed image processing, improvement and enhancement of the image contrast were attempted without increasing the imaging dose. To assess the feasibility of the image processing, portal images with and without the scatter compensation were compared.

2 | METHODS

2.A | The proposed image-processing algorithm

The original portal image is generated by primary and scatter photons that occur on the EPID. The signal P_o at the pixel coordinate (x, y) is the sum of the signals by primary photons $P_p(x, y)$ and scatter photons $P_s(x, y)$ as follows:

$$P_o(x, y) = P_p(x, y) + P_s(x, y) \quad (1)$$

To improve the image contrast, scatter photons must be eliminated. It has been reported that the signal of the EPID P is proportional to absorbed dose D to the scintillator.^{12,13} The $P_s(x, y)$ can be estimated using absorbed doses by primary photons $D_p(x, y)$ and scatter photons $D_s(x, y)$ as follows:

$$P_s(x, y) = P_o(x, y) \frac{D_s(x, y)}{D_p(x, y) + D_s(x, y)} \quad (2)$$

D_p and D_s can be calculated by using MC simulation in detail. Accordingly, the signal by primary photons $P_p(x, y)$ is calculated by the subtraction of $P_s(x, y)$ from $P_o(x, y)$,

$$P_p(x, y) = P_o(x, y) - P_s(x, y) \quad (3)$$

However, the entire EPID signal is weakened by the subtraction process. To enhance the image contrast without increasing the imaging dose, we propose a means of reusing the scatter photons that were eliminated by the subtraction process. Eliminated scatter photons are made to reproject from scattering points to the EPID as primary

photons on the assumption that Compton interaction did not take place. In consideration of the energy difference between the reprojecting photon $h\nu_r$ and the scatter photon $h\nu_s$, the signal by the reprojecting photon ΔP_r is estimated by the ratio of absorbed dose by the reprojecting photon $\Delta D(h\nu_r)$ to that by the scatter photon $\Delta D(h\nu_s)$.

$$\Delta P_r = \frac{\Delta D(h\nu_r)}{\Delta D(h\nu_s)} \Delta P_s, \quad (4)$$

where $\Delta D(h\nu_r)$ and $\Delta D(h\nu_s)$ are the absorbed dose to the scintillator by a photon with energy $h\nu_r$ and $h\nu_s$ respectively. They can be estimated by MC simulation for each photon. ΔP_s is the signal by a scatter photon that is calculated as follows:

$$\Delta P_s = \frac{\Delta D(h\nu_s)}{D_s} P_s \quad (5)$$

Then, the signal $P_r(x, y)$ by n reprojecting photons can be calculated by the summation of $\Delta P_r(x, y)$,

$$P_r(x, y) = \sum_{i=1}^n \Delta P_{r,i}(x, y) \quad (6)$$

Finally, the signal of the contrast enhanced image $P_c(x, y)$ is obtained by the sum of $P_p(x, y)$ and $P_r(x, y)$.

$$P_c(x, y) = P_p(x, y) + w \times P_r(x, y) \quad (7)$$

where w is the weight factor for adjustment of the contrast enhancement.

2.B | Simulation of absorbed dose to $Gd_2O_2S:Tb$ by a photon

Figure 1 shows the geometric arrangement of the EPID (Portal Vision a-S500 on Clinac 21 EX, Varian Medical System) for the simulation. The EPID was modeled in detail according to the design provided by the manufacturer. It is mainly composed of a copper (Cu) plate, terbium-doped gadolinium oxysulfide ($Gd_2O_2S:Tb$) scintillator and amorphous silicon (a-Si) photodiodes. The Cu plate filters lower energy photons and electrons; the Cu plate acts as the photons for the electrons converter when high-energy photons are impinged upon. Then, the scintillator generates fluorescence by electrons from

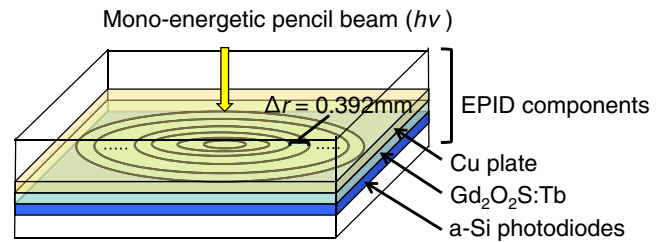


Fig. 1. Geometric arrangement of the EPID for the simulation. The EPID is mainly composed of a Cu plate, $Gd_2O_2S:Tb$ scintillator and a-Si photodiodes. In the simulation, equally spaced radial bins with $\Delta r = 0.392$ mm (1/2 of pixel width) were arranged, and the absorbed dose to $Gd_2O_2S:Tb$ by a photon from the EPID surface was simulated using the DOSRZnc code.

the Cu plate. It is estimated that 99.5% of the total signal is generated within the scintillator.¹³

Electron trajectories are complicated within the EPID. To that end, the absorbed dose to $\text{Gd}_2\text{O}_2\text{S:Tb}$ by a photon from the EPID surface was simulated using the DOSRZnrc code,¹⁴ and the dose spread functions of photon energy $h\nu$ and the radial distance from pencil beam r , $\Delta D(h\nu, r)$ were obtained. In the simulation, equally spaced radial bins with $\Delta r = 0.392$ mm (1/2 of pixel width) were arranged. The EPID consists of not only the main three layers but also low-density materials, such as air, paper and foamed body. In order to consider the spread of low-energy particles within low-density materials, the cut-off energies of photons and electrons were set to 10 and 521 keV.

2.C | Acquisition of portal image and 3D-CT image

The thorax phantom (N-1 LUNGMAN, Kyoto Kagaku) was modeled as a patient. A water-equivalent 2 cm ϕ sphere was inserted into the right lung as a tumor. The original portal image was acquired with 6 MV therapeutic beam of a linac (Clinac 21EX, Varian Medical System). The thorax phantom was irradiated with 5 monitor units. The source to the axis distance (SAD) and source to the EPID distance (SDD) were 1000 and 1400 mm, respectively. The field size was set to 40 cm \times 30 cm at the EPID, which has 512 \times 384 pixels, the pixel size was 0.784 mm \times 0.784 mm and the signals were recorded as a 16-bit integer.

The 3D-CT data were obtained by the SPECT-CT scanner (Symbia T2, Seimens Healthcare) with the reconstruction matrix 512 \times 512 \times 512 and voxel size of 0.7 mm \times 0.7 mm \times 1.0 mm.

2.D | Photon sampling and image processing

3D-CT data of the thorax phantom was modeled in EGS5 to investigate photon trajectories in detail.¹⁵ Figure 2 shows a simplified diagram of the photon sampling. The simulation geometry, e.g., SAD,

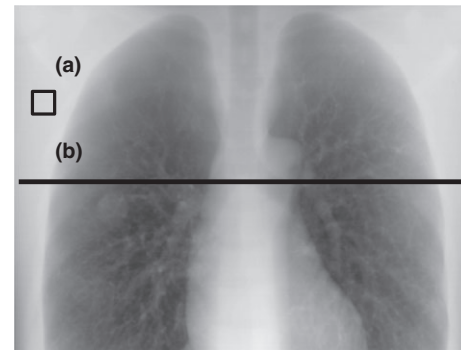
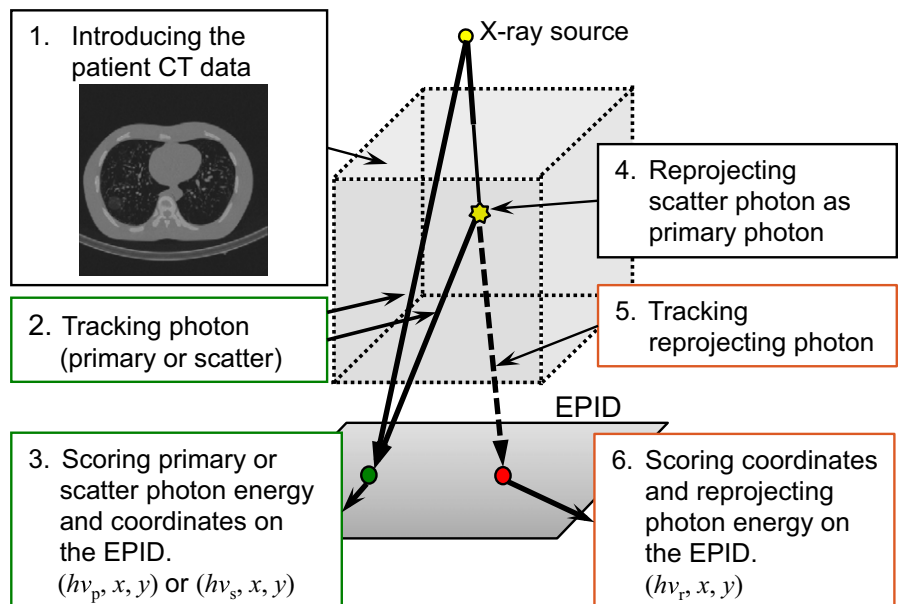


FIG. 3. (a) Reference region (square area) and (b) line profile for the image contrast evaluation. The reference region was selected as the homogeneous background in the portal image. The image contrast profile $C(x, y)$ was evaluated along the line profile.

SDD, and field size, was the same as the MV portal imaging described in 2.C. A 6 MV beam was reproduced according to the energy spectrum. When the photon reached the EPID surface, the coordinates (x, y) and energy $h\nu$ of primary and scatter photons were sampled. Additionally, if it was a scatter photon, the coordinates (x, y) and energy $h\nu_r$ of the reprojecting photon were sampled on the assumption that the Compton interaction does not take place.

To calculate the absorbed dose D for each pixel, the deposit energy was sampled within r away from the incident point (x, y) according to the dose spread function $\Delta D(h\nu, r)$. Thus, $D_s(x, y)$ and $D_p(x, y)$ for each pixel were calculated by accumulation of the dose spread by scatter and primary photons, respectively. In the subtraction process, $P_s(x, y)$ and $P_p(x, y)$ were obtained according to eqs. (2) and (3). In the reprojecting process, signals by a scatter photon ΔP_s were calculated using $\Delta D(h\nu, r)$ and the signal by the reprojecting photon ΔP_r was calculated by eq. (4) but $\Delta D(h\nu_r)/\Delta D(h\nu_s)$ was replaced with $\Delta D(h\nu_r, r)/\Delta D(h\nu_s, r)$ in consideration of the dose spread. The image processing code was developed using the Qt 5.2.1 toolkit and the code was written in C++.

FIG. 2. Simplified diagram of the photon sampling for the image processing. The simulation geometry was the same as the MV portal imaging. 3D-CT data of the thorax phantom was modeled as a patient. A 6 MV beam was reproduced and photon trajectories were investigated in detail. When the photon reached the EPID surface, the coordinates (x, y) and energy of primary and scatter photons, $h\nu_p$ and $h\nu_s$, were sampled. If it was a scatter photon, the coordinates (x, y) and energy $h\nu_r$ of the reprojecting photon were sampled on the assumption that the Compton interaction does not take place.



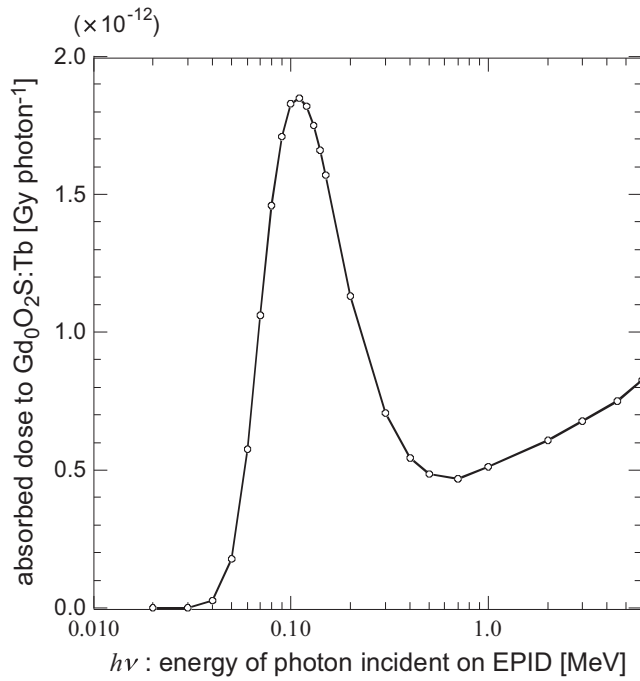


FIG. 4. Absorbed dose to the $\text{Gd}_2\text{O}_2\text{S:Tb}$, $\Delta D(h\nu, 0)$, as a function of photon energy.

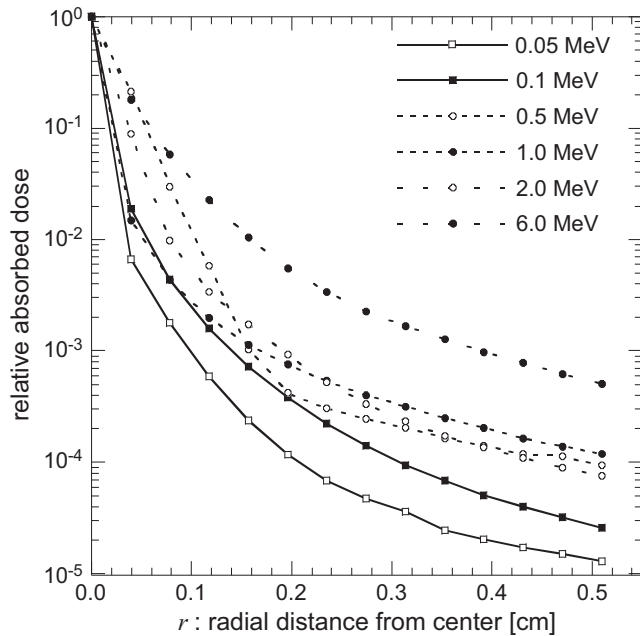


FIG. 5. Dose spread functions of $\Delta D(h\nu, r)$ as a function of photon energy and radial distance from pencil beam.

2.E | Evaluation of portal images with and without the image processing

The portal images with and without the proposed image processing were evaluated by the image contrast profile $C(x, y)$ that was used by Kairn et al¹⁶. $C(x, y)$ was calculated by the following equation:

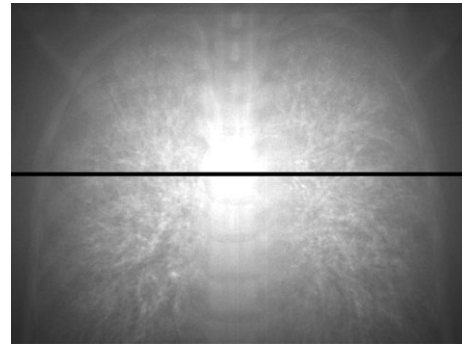


FIG. 6. Portal image generated by scatter photons only (P_s image). Signal profile was obtained along the solid line.

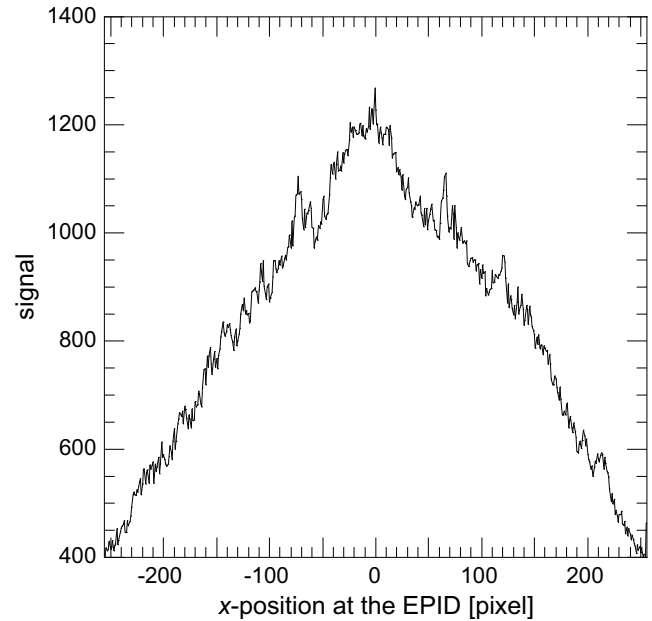


FIG. 7. Signal profile along the solid line at the P_s image.

$$C(x, y) = \frac{P(x, y) - P_{\text{ref}}}{P_{\text{ref}}}, \quad (8)$$

where P_{ref} is the mean signal of the reference region that is indicated as a square in Fig. 3(a). The reference region was selected as the homogeneous background in the portal image. $C(x, y)$ was evaluated along the line profile shown in Fig. 3(b).

3 | RESULTS

3.A | Absorbed dose to $\text{Gd}_2\text{O}_2\text{S:Tb}$ by a photon

Figure 4 shows the absorbed dose to the $\text{Gd}_2\text{O}_2\text{S:Tb}$ at $r = 0$, $\Delta D(h\nu, 0)$, as a function of photon energy. When $h\nu$ was lower than 0.7 MeV, $\Delta D(h\nu, 0)$ became maximum at $h\nu = 110$ keV and decreased quickly with the decrease in $h\nu$. On the other hand, when $h\nu$ was greater than 0.7 MeV, $\Delta D(h\nu, 0)$ increased slowly with the increase in $h\nu$. This tendency suggests that the Cu plate acted as a

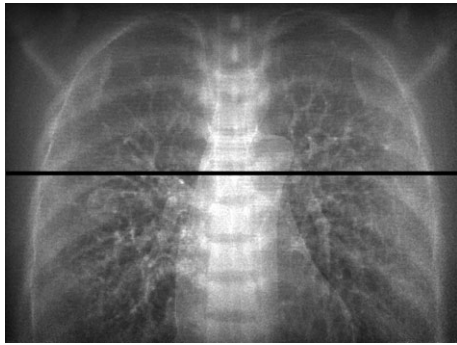


FIG. 8. Portal image generated by reprojecting photons only (P_r image). Signal profile was obtained along the solid line.

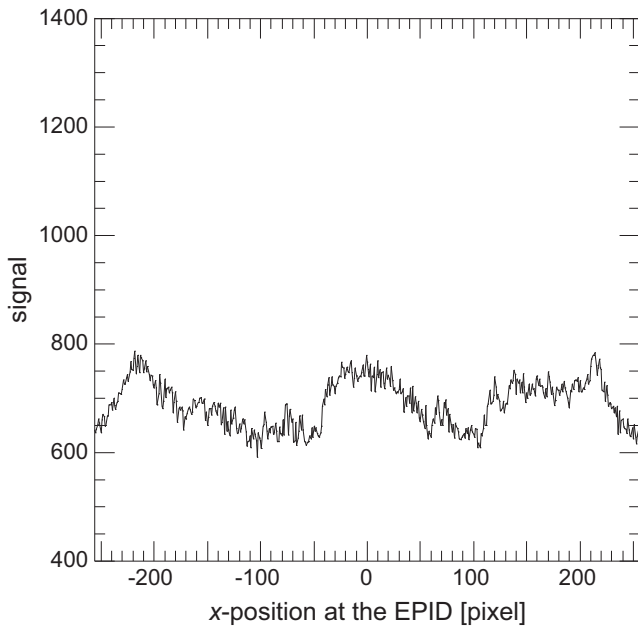


FIG. 9. Signal profile along the solid line at the P_r image.

buildup plate and the large number of recoil electrons reached the $\text{Gd}_2\text{O}_2\text{S:Tb}$.

Figure 5 shows dose spread functions $\Delta D(h\nu, r)$ that normalized to absorbed dose at $r = 0$, $\Delta D(h\nu, 0)$. It was observed that the

contribution of the dose spread was increased with the increase in $h\nu$, and this phenomenon was not negligible in MV imaging. The ratio of $\Delta D(h\nu, r)$ to $\Delta D(h\nu, 0)$ was lower than 0.5% when $h\nu$ was lower than 1.0 MeV and r exceeds 2.5 mm. Accordingly, in the image processing code, $\Delta D(h\nu, r)$ calculations were performed in $0.0 \text{ mm} \leq r \leq 2.5 \text{ mm}$.

3.B | Evaluation of portal image with and without the proposed image processing

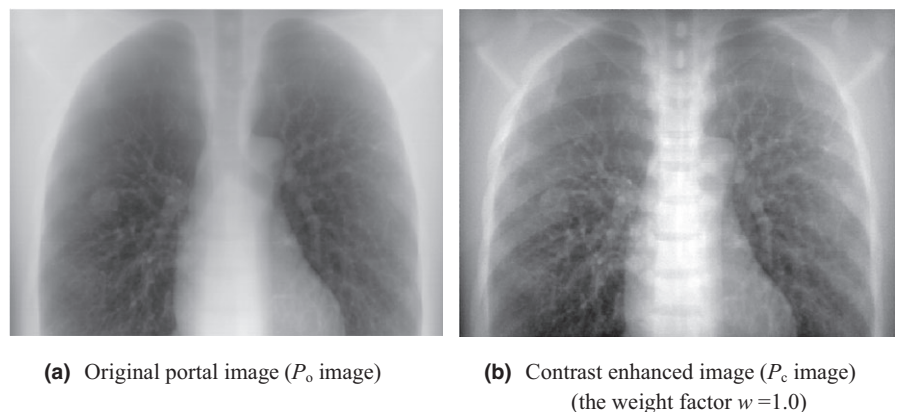
Figure 6 shows the portal image of the thorax phantom by scatter photons only (P_s image) and Fig. 7 shows the signal profile along the solid line at the P_s image. The signal by scatter photons was increased near the center of the image. For the 6 MV X-ray beam, it was clarified that 15.2% of whole EPID signal was generated by scatter photons. Primary photons were mainly scattered in bone structures and the mediastinal space, then the contribution of scattered photons became larger in the center of the EPID. Figure 8 shows the portal image of the thorax phantom by reprojecting photons only (P_r image) and Fig. 9 shows the signal profile along the solid line at the P_r image. The convex profile by scatter photons indicated in Fig. 7 was corrected and the thorax structures could be observed by reprojecting photons.

Figure 10 shows a comparison between the original portal image (P_o image) and the contrast enhanced image (P_c image) that has the weight factor $w = 1.0$. Two images were displayed with the same window width, and gray levels were adjusted to be the same at the coordinates ($x = 257$, $y = 26$) where the spinous process was observed. As a result, the thorax structures, e.g., the tumor, bronchi, mediastinal space and ribs were observed more clearly in the P_c than in the P_o image. Figure 11 shows a comparison of contrast profiles between P_o , P_p and P_c images. The image contrast of the P_c image was superior to other images.

4 | DISCUSSION

Compton interaction becomes dominant above 30 keV for soft tissues and above 60 keV for bone. Within the thorax phantom, most

FIG. 10. Comparison between original image (P_o image) and contrast enhanced image (P_c image). Two images were displayed with the same window width, and gray levels were adjusted to be the same at the coordinates ($x = 257$, $y = 26$) where the spinous process was observed.



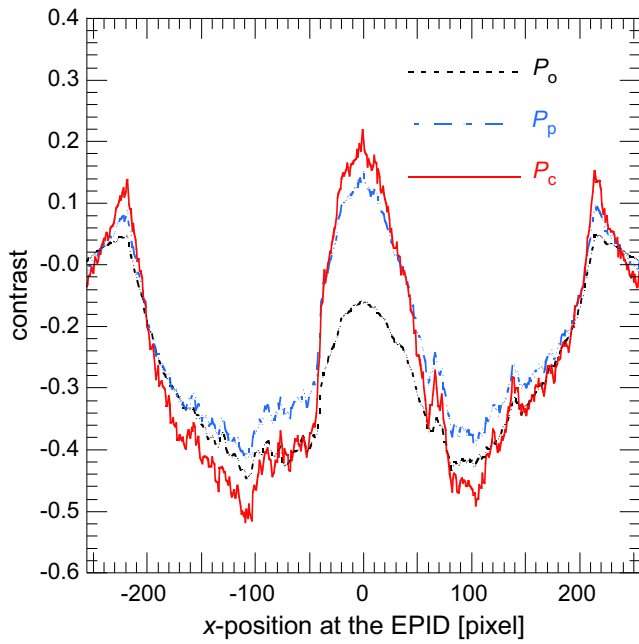


FIG. 11. Comparison of contrast profiles between P_o , P_p , and P_c images. The contrast profile was calculated by using the reference region and the line profile as shown in Fig. 3. The dotted line, dashed-dotted line and solid line expressed contrast profiles in P_o , P_p , and P_c images respectively.

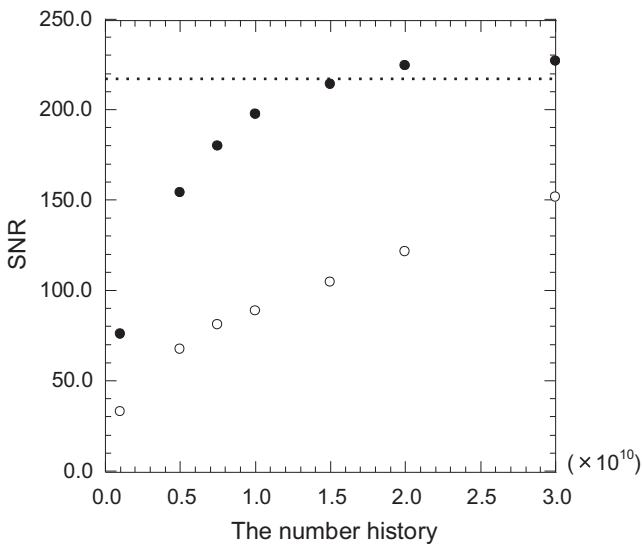


FIG. 12. SNR in the reference region of the P_c image as a function of the number history. Filled and open circles represent the image processing with and without the dose spread functions. The dotted line expresses SNR of the original portal image.

of the interaction was Compton scattering for the 6 MV X-ray beam. By the MC simulation, it was calcified that 15.2% of the EPID signal was generated by scatter photons. Therefore, it is confirmed that image processing against scatter photons is required for MV imaging.

The proposed image processing was performed by the combination of the subtraction and the reprojection processes. The number of scatter photons increased as the density of the structure

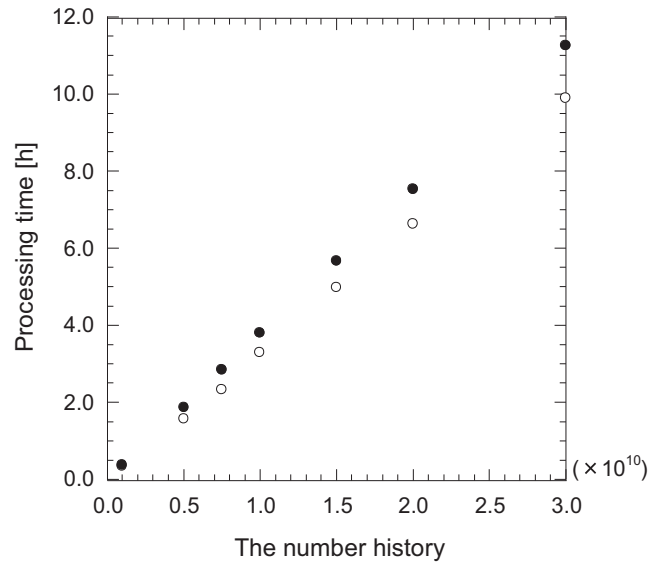


FIG. 13. Processing time as a function of the number history. Filled and open circles represent the image processing with and without the dose spread functions.

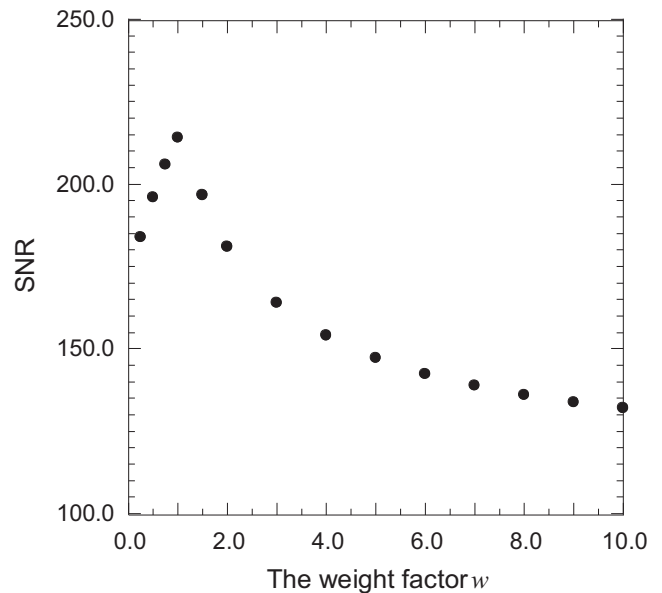
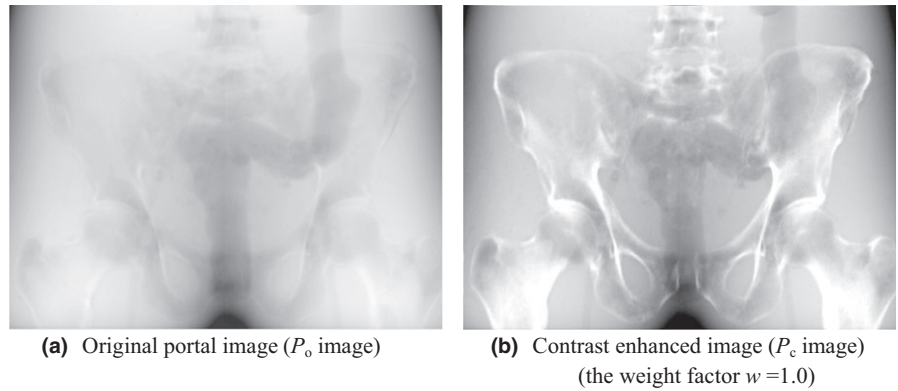


FIG. 14. SNR in the reference region of the P_c image as a function of the weight factor w . The SNR increased until $w = 1.0$, then the SNR decreased with the increase in w .

increased. Even with the weight factor w being 0, namely without the reprojection process, the image contrast was improved. On the other hand, the EPID signal was weakened because 15.2% of the signal was eliminated as the contribution of scatter photons by the subtraction process. Hence, these scatter photons were reprojected as primary photons in the reprojection process. Consequently, it was clarified that scatter photons were utilized as primary photons for more contrast enhancement without increasing the imaging dose.

The proposed image processing includes the photon sampling process using the MC simulation. Thus, the signal-to-noise ratio

FIG. 15. Pelvis phantom images with/without the proposed image processing. Two images were displayed with the same window width, and gray levels were adjusted to be the same at the coordinates ($x = 256, y = 20$) between vertebral bodies. The contrast enhanced image with sufficient SNR was obtained when the number history was 1.0×10^{10} .



(SNR) of the contrast enhanced image depends on the number history. To improve the photon sampling efficiency, the electron tracking was discarded in this work because the electrons from the thorax phantom reaching the EPID might be disregarded. As a result, the processing time of the photon sampling was shortened by approximately 1/27. The absorbed dose within the EPID was not calculated by the MC simulation but by using the dose spread function. Figure 12 shows SNR as a function of the number history in the reference region of the P_c image. The SNR of the P_c image by using the dose spread function reached that of the original portal image when the number history was more than 1.5×10^{10} . On the other hand, the SNR without the dose spread function was 2/3 in spite of the number history being 3.0×10^{10} . Figure 13 shows the whole processing time as a function of the number history. The time of processing by using the dose spread function increased less than 10% although the SNR was improved. It was clarified that the image processing with the dose spread functions achieves contrast enhancement while maintaining sufficient SNR.

The weight factor w amplifies the signal of the reprojecting photons according to eq. (7). On the other hand, there are concerns about the noise enhancement caused by insufficient statistics in MC simulation. Figure 14 shows the SNR as a function of the weight factor w in the reference region of the P_c image. The SNR increased until $w = 1.0$, then SNR decreased with increase in w . The SNR is improved by increasing the number history but it takes a longer processing time. Hence, to observe the thorax structures clearly while reducing the processing time, the optimal weight factor and sufficient number history are 1.0 and 1.5×10^{10} respectively.

For other treatment site, the optimal parameters, i.e. the weight factor and the number history, could be different. As an example, Fig. 15 shows portal images of a pelvis phantom (Sectional Lower Torso Phantom, The Phantom Laboratory) with and without the proposed image processing. When the weight factor w was 1.0, bone structures were enhanced and a hollow cavity that reproduced the diverticulum and rectum were observed clearly. Since large amount of Compton scatter photons from pelvis were reprojected as primary, sufficient SNR was obtained when the number history was 1.0×10^{10} . Although the density, location and volume of structures within the pelvis are different from that within the thorax, it was confirmed that contrast enhanced images can be obtained with same

weight factor. Therefore, the proposed image processing might be available for major treatment sites with the weight factor $w = 1.0$ and at least 1.5×10^{10} histories.

Further works, e.g., speedup of the image processing using the graphics processing units (GPU) based MC simulation,¹⁷ investigation of optimal parameters considering patient's size and image registration adapting temporal changes in anatomy, are necessary to raise the possibilities and reduce the limitations of the proposed image processing.

5 | CONCLUSION

Original image processing was proposed to improve and enhance the contrast of portal images. In the image processing, a combination of the subtraction and reprojection processes was performed using the photon sampling data. To improve the processing efficiency, the dose spread functions within the EPID were investigated and implemented on the developed code. In the contrast enhanced image, the structures were observed more clearly than in the original portal image. Consequently, this work demonstrates the feasibility of improving and enhancing the contrast of portal images.

ACKNOWLEDGMENT

This work was supported by a grant-in-aid (GC215, 2016) for research on priority areas of Tokyo Metropolitan University.

CONFLICT OF INTEREST

The authors declare no conflict of interest.

REFERENCES

- Murphy MJ, Balter J, Balter S, et al. The management of imaging dose during image-guided radiotherapy: report of the AAPM Task Group 75. *Med Phys.* 2007;34:4041–4063. <https://doi.org/10.1118/1.2775667>.
- Bissonnette J-P, Balter PA, Dong L, et al. Quality assurance for image-guided radiation therapy utilizing CT-based technologies: a report of the AAPM TG-179. *Med Phys.* 2012;39:1946–1963. <https://doi.org/10.1118/1.3690466>.

3. Jaffray DA, Drake DG, Moreau M, Martinez AA, Wong JW. A radiographic and tomographic imaging system integrated into a medical linear accelerator for localization of bone and soft-tissue targets. *Int J Radiat Oncol*. 1999;45:773–789. [https://doi.org/10.1016/S0360-3016\(99\)00118-2](https://doi.org/10.1016/S0360-3016(99)00118-2).
4. Sharpe MB, Moseley DJ, Purdie TG, Islam M, Siewerdsen JH, Jaffray DA. The stability of mechanical calibration for a kV cone beam computed tomography system integrated with linear accelerator. *Med Phys*. 2006;33:136–144. <https://doi.org/10.1118/1.2143141>.
5. Yoo S, Kim G-Y, Hammoud R, et al. A quality assurance program for the on-board imagers. *Med Phys*. 2006;33:4431–4447. <https://doi.org/10.1118/1.2362872>.
6. Xing L, Chang J, Orton CG, Xing L, Ph D. Kilovoltage imaging is more suitable than megavoltage imaging for guiding radiation therapy. *Med Phys*. 2007;34:4563–4566. <https://doi.org/10.1118/1.2799489>.
7. American Association of Physicists in Medicine (AAPM). The role of in-room kV X-Ray imaging for patient setup and target localization report of AAPM task group 104. Report of Task Group 104 of the Therapy Imaging Committee. 2009;1–62.
8. Samant SS, Gopal A. Analysis of the kinesthetic charge detection system as a high detective quantum efficiency electronic portal imaging device. *Med Phys*. 2006;33:3557–3567. <https://doi.org/10.1118/1.2241991>.
9. Ruhrschopf E-P, Klingensbeck K. A general framework and review of scatter correction methods in X-ray cone-beam computerized tomography. Part 1: scatter compensation approaches. *Med Phys*. 2011;38:4296–4311. <https://doi.org/10.1118/1.3589140>.
10. Ruhrschopf E-P, Klingensbeck K. A general framework and review of scatter correction methods in cone beam CT. Part 2: scatter estimation approaches. *Med Phys*. 2011;38:5186–5199. <https://doi.org/10.1118/1.3589140>.
11. Hansen VN, Swindell W, Evans PM. Extraction of primary signal from EPIDs using only forward convolution. *Med Phys*. 1997;24:1477–1484. <https://doi.org/10.1118/1.598036>.
12. Antonuk LE, El-Mohri Y, Huang W, et al. Initial performance evaluation of an indirect-detection, active matrix flat-panel imager (AMFPI) prototype for megavoltage imaging. *Int J Radiat Oncol Biol Phys*. 1998;42:437–454.
13. Munro P, Bouiuis DC. X-ray quantum limited portal imaging using amorphous silicon flat-panel arrays. *Med Phys*. 1998;25:689–702. <https://doi.org/10.1118/1.598252>.
14. Kawrakow I, Mainegra-Hing E, Rogers DWO, et al. *The EGSnrc Code System: Monte Carlo Simulation of Electron and Photon Transport*. NRCC Technical Report PIRS-701. Ottawa, Canada: National Research Council of Canada; 2000.
15. Hirayama H, Namito Y, Bielajew AF, et al. *The EGS5 Code System. KEK Report 2005-8*. Tsukuba-shi, Japan: High Energy Accelerator Research Organization (KEK); 2005.
16. Kairn T, Khoei S, Markwell TS, et al. Contrast enhancement of EPID images via difference imaging: a feasibility study. *Phys Med Biol*. 2010;55:N533–N545. <https://doi.org/10.1088/0031-9155/55/22/N02>.
17. Lippuner J, Elbakri IA. A GPU implementation of EGSnrc's Monte Carlo photon transport for imaging applications. *Phys Med Biol*. 2011;56:7145–7162. <https://doi.org/10.1088/0031-9155/56/22/010>.